SOIL, 11, 535–552, 2025
https://doi.org/10.5194/soil-11-535-2025

SOIL Open Access EGU

Interplay of coprecipitation and adsorption processes: deciphering amorphous mineral–organic associations under both forest and cropland conditions

Floriane Jamoteau[1,2,3,4], Emmanuel Doelsch[2,3], Nithavong Cam[1], Clément Levard[1], Thierry Woignier[5,6], Adrien Boulineau[7], Francois Saint-Antonin[7], Sufal Swaraj[8], Ghislain Gassier[1], Adrien Duvivier[1], Daniel Borschneck[1], Marie-Laure Pons[1], Perrine Chaurand[1], Vladimir Vidal[1], Nicolas Brouilly[9], and Isabelle Basile-Doelsch[1]

[1]Aix Marseille Université, CNRS, IRD, INRAE, Coll France, CEREGE, Aix-en-Provence, 13545, France
[2]CIRAD, UPR Recyclage et risque, Montpellier, 34398, France
[3]Recyclage et Risque, Univ Montpellier, CIRAD, Montpellier, 34398, France
[4]Institute of Earth Surface Dynamics, University of Lausanne, Lausanne, 1015, Switzerland
[5]Campus Agro Environnemental Caraïbes-IMBE-CNRS, B.P. 214, Petit Morne, Le Lamentin, Martinique, 97232, France
[6]Laboratoire Charles Coulomb UMR 5221 CNRS-UM2, Université Montpellier 2, Montpellier CEDEX 5, 34095, France
[7]Université Grenoble Alpes, CEA, LITEN, Grenoble, 38100, France
[8]Synchrotron SOLEIL, L'Orme des Merisiers, Departementale 128, Saint-Aubin, 91190, France
[9]Aix-Marseille Université, CNRS UMR 7288, IBDM, Marseille, 13000, France

Correspondence: Floriane Jamoteau (floriane.jamoteau@unil.ch, jamoteau@cerege.fr)

Received: 19 September 2024 – Discussion started: 30 September 2024
Revised: 5 April 2025 – Accepted: 11 April 2025 – Published: 17 July 2025

Abstract. Mineral–organic associations are crucial carbon and nutrient reservoirs in soils. However, conversion from forest to agricultural systems disrupts these associations, leading to carbon loss and reduced soil fertility in croplands. Identifying the types of mineral–organic associations within a single soil is already challenging, and detecting those susceptible to disruption during forest-to-crop conversion is even more complex. Yet, addressing this identification challenge is essential for devising strategies to preserve organic matter in croplands. Here, we aimed to identify the predominant mineral–organic associations within an Andosol (developed on Fe-poor parent material) under both forest and cropland conditions. To achieve this, we collected Andosol samples from both a forested and a cultivated area, located 300 m apart. We then analyzed differences between the two soil profiles in soil physicochemical parameters and characterized mineral–organic associations using an array of spectro-microscopic techniques for comprehensive structural and compositional analysis. At microscale and nanoscale spatial resolution, we observed mineral–organic associations in the form of amorphous coprecipitates, composed of a mix of C+Al+Si and C+Al+Fe+Si nanoCLICs (inorganic oligomers with organics), proto-imogolites and organic matter, some Fe nanophases associated with organic matter, and some metal–organic complexes. This challenges prior conceptions of mineral–organic associations in Andosols by demonstrating the presence of amorphous coprecipitates rather than solely organic matter associated with short-range-order minerals (i.e., imogolite and allophanes). Moreover, chemical mappings suggested that these amorphous coprecipitates may adhere to mineral surfaces (i.e., phyllosilicates and imogolites), revealing secondary interactions of mineral–organic associations in soils. While the presence of similar amorphous coprecipitates in both the forest and crop Andosols was confirmed, the crop soil had 75 % less C in mineral–organic associations (in the 0–30 cm depth). Although the sample size for comparing land use types is limited, these results suggest that the nature of mineral–organic associations remains identical despite quantitative differences. This study highlights the crucial role of

amorphous coprecipitates in C stabilization in Andosols and also suggests their vulnerability to disruption after 30 years of a forest-to-crop conversion, thereby challenging our understanding of the persistence of mineral–organic associations in Andosols.

1 Introduction

Carbon sequestration in terrestrial ecosystems is facilitated by protecting organic compounds within mineral–organic associations from microbial access (Cotrufo et al., 2019; Lugato et al., 2021). Beyond their contribution to carbon sequestration, these associations serve as crucial nutrient reserves for plants and soil microorganisms, thereby enhancing soil fertility, which is essential for maintaining agricultural productivity (Bernard et al., 2022; Fontaine et al., 2024). However, soil cultivation disrupts these mineral–organic associations, leading to significant loss of C – a phenomenon known as "C destabilization" (Sanderman et al., 2017; Bailey et al., 2019). In order to maintain agricultural productivity in cultivated soils, it is essential to preserve mineral–organic associations in croplands.

Mineral–organic associations have traditionally been regarded as resulting from organic matter adsorption onto mineral surfaces or coprecipitation of organic compounds with weathered elements from minerals (Basile-Doelsch et al., 2015). In soil with neutral to acidic pH, the predominant mineral–organic associations can include organic matter associated with short-range-order minerals (e.g., ferrihydrite, imogolites, allophanes; Fig. 1) or metal–organic complexes (Wagai and Mayer, 2007; Kleber et al., 2015; Chen et al., 2014; Rasmussen et al., 2018; Basile-Doelsch et al., 2020; Kleber et al., 2021). Yet, measuring the exact mineral composition of mineral–organic associations is difficult to achieve and largely stems from indirect measurements of minerals rather than direct characterizations of the entire mineral–organic assemblage (e.g., using selective extractions; Rennert and Lenhardt, 2024). Recent advances in nanoscale (spectro-)microscopy (e.g., transmission election microscopy coupled with energy-dispersive X-ray spectroscopy – TEM-EDX, scanning transmission X-ray microscopy – STXM) have facilitated precise analyses of mineral–organic associations' composition and structure (Kinyangi et al., 2006; Solomon et al., 2007; Wan et al., 2007; Solomon et al., 2012; Asano et al., 2018), offering deeper insights into mineral–organic association composition. In Andosols, i.e., soils with high concentrations of mineral–organic associations, microscopy and spectroscopy analyses raised questions about the stabilizing role of short-range-order minerals in the form of imogolite or allophane for C (Levard et al., 2012). Instead, organic C was primarily associated in the form of nanosized coprecipitates of inorganic oligomers with organics (nanoCLICs). In such structures, organic molecules are linked to a few atoms of Al, Fe, or Si without crystalline structures (Tamrat et al., 2018, 2019; Jamoteau et al., 2023). These nanoCLICs phases do not fit into the spectra of metal–organic complexes because they are more heterogeneous in composition (Al, Fe, Si, and some Ca, Mg, K, etc.) and organic molecules are linked to metallic oligomers of approximately 2–3 atoms (Tamrat et al., 2019; Jamoteau et al., 2023). These findings challenge previous assumptions about the types of mineral–organic associations in Andosols developed from basalt parent material and suggest that, in some situations, an Andosol's mineral–organic associations may contain a more amorphous structure than earlier proposed models of short-range-ordered minerals (Jamoteau et al., 2023). The presence of nanoCLICs rather than short-range-order minerals with organic matter in Andosols derived from basaltic parent material could be explained by two hypotheses: either organic matter directly associates with amorphous phases to form nanoCLICs instead of short-range-order minerals, or the presence of Fe in the soil solution (derived from the weathering of basaltic parent material) prevents Al and Si from assembling into short-range-order minerals like imogolite and allophane. In sum, these studies, showing various types of mineral–organic associations in different Andosols, now raise the question of their coexistence within the same soil and whether some types of associations are predominant. To determine if nanoCLICs, short-range-ordered minerals with adsorbed organic matter ,and metal–organic complexes coexist in Andosols or if one type is more prevalent, further nanoscale characterization of mineral–organic associations in Andosol is required.

In addition to characterizing existing mineral–organic associations, identifying the ones vulnerable to destruction or transformation during forest-to-crop transition is crucial for developing strategies to preserve organic matter in croplands. Disruption of mineral–organic associations in crop soils can be attributed to multiple factors: (i) disruption of soil aggregates, releasing entrapped mineral–organic associations (Bailey et al., 2019; Derrien et al., 2023; Even and Cotrufo, 2024); (ii) intensified root and microbial activities within cropping systems, accelerating mineral–organic association disruption through priming effects (Keiluweit et al., 2015; Jilling et al., 2021; Fontaine et al., 2024); or (iii) shifts in soil physicochemical parameters, notably pH, weakening mineral–organic interactions (Newcomb et al., 2017; Bailey et al., 2019). However, regardless of these factors, the susceptibility of mineral–organic associations to disruption varies, depending on mineral crystallinity and binding strength (Li et al., 2017; Newcomb et al., 2017; Bernard et al., 2022). Consequently, some associations could be more prone to disrup-

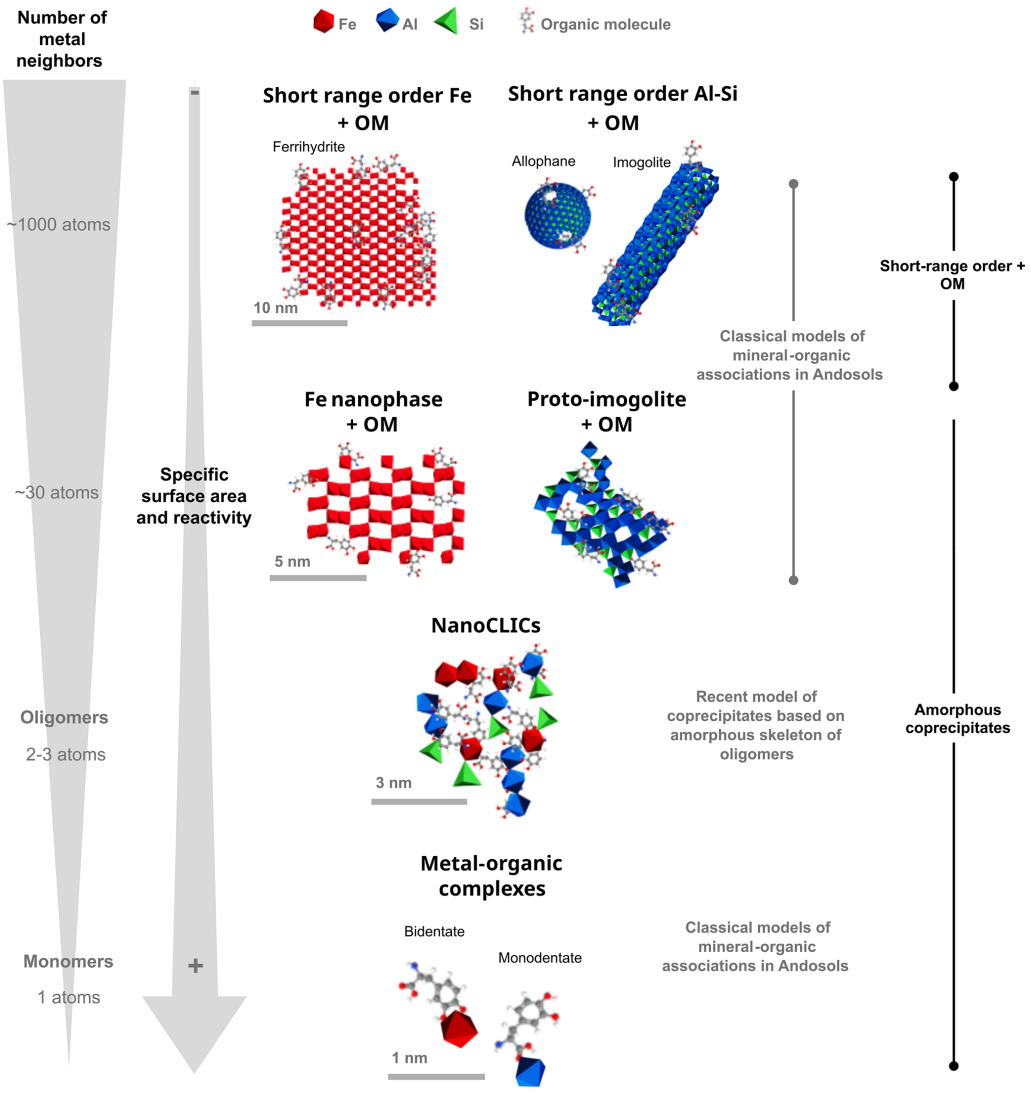

Figure 1. Molecular models of mineral–organic associations in Andosols. Mineral–organic associations can be described as follows: (i) an inorganic phase consisting of clusters of 100 to 1000 atoms, forming an organized crystal structure known as short-range-order minerals (SROs) – these SROs include ferrihydrite (composed of Fe; representation adapted from Kleber et al., 2015), imogolites, or allophanes (composed of Si and Al; representation adapted from Levard et al., 2012); (ii) an inorganic phase with approximately 30 atoms showing limited atomic organization at the local scale, such as Fe nanophases (adapted from Kleber et al., 2015) and proto-imogolites (adapted from Levard et al., 2012); (iii) an inorganic phase with small amorphous oligomers formed by the polymerization of 2–3 atoms of Al, Fe, and Si, without local arrangement, referred to as nanoCLICs (adapted from Tamrat et al., 2019 and Jamoteau et al., 2023); and (iv) an inorganic component involving a single monomer (e.g., Fe, Al) complexed with organic molecules.

tion than others, potentially altering the types of remaining mineral–organic associations after long-term soil cropping. Although the underlying mechanisms are not fully understood, some evidence suggests that associations with lower mineral crystallinity are particularly prone to disruption and exhibit faster turnover (Li et al., 2017; Hall et al., 2018). In Andosols, for instance, nanoCLICs-type mineral–organic associations, characterized by their amorphous mineral components composed of only a few atoms, could be particularly prone to disruption. Therefore, long-term cropping of Andosols may lead to the disruption of nanoCLICs-type associations, which would significantly alter the type of remaining mineral–organic associations.

This study aims to (i) identify the predominant mineral–organic associations within an Andosol (developed on Fe-poor parent material) under both forest and cropland conditions, as well as to explore possible differences in the types of mineral–organic associations, and (ii) to determine if mineral–organic associations in a forested Andosol developed on Fe-poor parent material (andesite) are similar

to mineral–organic associations in a forested Andosol developed on Fe-rich parent material (basalt; from Jamoteau et al., 2023). Our working hypotheses posit that (i) organic matter preferentially associates with amorphous mineral phases rather than short-range-order minerals in relatively young Andosols (< 100 kyr) developed on Fe-poor parent material, and (ii) nanoCLICs are particularly prone to physicochemical transformations induced by cultivation, making them susceptible to destruction and shifting the predominant mineral–organic association in the cultivated Andosol from nanoCLICs-type to adsorption of organic matter onto short-range-order minerals. To probe these hypotheses, we sampled an Andosol formed on an Fe-poor parent material (andesite parent material). We conducted analyses on two Andosol topsoils that are 300 m apart, one under forest and the other subjected to 3 decades of cultivation. We then identified differences between the forest and crop soil profiles in physicochemical parameters and characterized mineral–organic associations by employing an array of spectro-microscopic techniques including TEM-EDX, TEM-EELS (transmission electron microscopy coupled with electron energy loss spectroscopy), and STXM for comprehensive structural and compositional analysis. Although only single profiles per land use type were compared (limiting broader site-level or land use comparisons), this approach was chosen to enable high-resolution imaging and direct visualization of mineral–organic associations.

2 Material and methods

2.1 Soil sampling

Two Andosol profiles were sampled on La Martinique island (French West Indies), formed a few hundred years ago (with the most recent volcanic eruption in 1929) on andesite parent material. One profile was located under a forest (14°46′31″ N; 61°2′31″ W), while the other was situated 300 m away in an area converted to agriculture 30 years ago (14°46′27″ N; 61°2′57″ W). Both profiles were situated on a flat area at 300 m above sea level in a humid tropical climate (average temperature of 25 °C and average annual precipitation of 3000 mm yr^{-1}). The crop soil, converted 30 years ago, transitioned from a forest to a banana plantation followed by a cropping system with 3-year rotations of taro, sweet potatoes, yams, and fallow periods. During the crop rotation system, plowing was carried out to a depth of 30 to 40 cm. The differences observed between these two soil profiles may primarily result from their different land uses: one soil has remained in a forest for 30 years, while the other has been converted for agriculture. Soil sampling was carried out by opening soil pits and subsequently sampling three samples per soil horizon (on different sides of the pits), for a total sampling of ∼ 1 kg of soil per horizon (i.e., at 0–5, 5–10, 10–20, 20–30, 30–40, 40–50, 50–60, 60–70, 70–80 cm). After sampling, the samples were kept humid at 4 °C.

2.2 Monitoring differences in soil physicochemical parameters between the forest and crop soils

To monitor differences between the forest and the crop Andosol profiles, analyses of bulk soils and fine fractions (primarily composed of C in the form of mineral–organic associations) were carried out. The fine fractions from both soils were isolated through wet sieving: briefly, 10–20 g of air-dried soil was added to 100 mL of Milli-Q water and sonicated (16 J mL^{-1}). The 100 mL suspension was then wet-sieved using a 20 µm mesh. After a minimum 12 h settling period at 4 °C of the < 20 µm fraction, the supernatant was removed, and the sedimented fraction was dried at 30 °C.

The C content of bulk soils and fine fractions was analyzed using dry combustion with a Thermo FlashSmart elemental analyzer. The mineralogy of bulk soils and fine fractions was analyzed on free powder deposited on a silicon sample holder. This analysis was performed using an X-ray diffractometer (Co-Kα source at 40 mA; $\lambda = 1.79$; 2–75°; time step of 0.033°, Philips P3710 X-ray). The quantity of poorly crystalline phases in bulk soils was quantified through sequential extractions using Na-pyrophosphate, ammonium oxalate acid, and dithionite–citrate bicarbonate (Tamm, 1922; Pansu and Gautheyrou, 2006). After extractions, solubilized Fe, Al, and Si were measured using inductively coupled plasma atomic emission spectroscopy (ICP-AES).

Soil organic carbon stocks (SOC stocks, kg m^{-2}) were calculated using the following equation (Poeplau et al., 2017; Quéro et al., 2021):

$$\text{SOC stock}_i = \text{BD}_i \times \text{TOC}_i \times e_i / 10, \quad (1)$$

where i refers to the considered soil horizon, and n is the number of analyzed horizons. TOC represents the soil carbon concentration [g kg^{-1}], BD is the bulk density [g cm^{-3}], and e is the layer thickness [cm]. A correction was applied to compare cumulated C stocks at equivalent mass, avoiding differences in bulk density between the two sites for the same depth (Ellert and Bettany, 1995; Poeplau et al., 2017). The reference soil mass was the heaviest horizon. This correction of the C stock (SOC equivalent_mass) was applied to all cumulative horizons from 0 to 80 cm, following Eq. (2):

$$\text{SOC stock}_{\text{equivalent\_mass}} = \text{SOC stock}_n + \left(\text{TOC}_{n+1} \cdot \frac{M_{n\ \text{heaviest}} - M_n}{10}\right), \quad (2)$$

where n is the considered horizon, SOC stock_n is the uncorrected cumulative SOC stock in kg m^{-2}, $M_{n\ \text{heaviest}}$ is the heaviest soil mass [g cm^{-2}] of the two sites, M_n is the lightest soil mass [g cm^{-2}], and TOC is the soil C concentration.

2.3 Characterization of mineral–organic associations

2.3.1 Probing types of mineral–organic associations using TEM images and TEM-EDX and TEM-EELS chemical mappings

For microscopy analyses, fine fractions of the forest and the crop soil were isolated through sedimentation: 2 g of soil from the 10–20 cm horizon was added to 35 mL of Milli-Q water and sonicated at low power to induce minimal disaggregation (16 J mL^{-1}; Just et al., 2021). After a minimum of 1 h of sedimentation, the brown supernatant (with a gel-like texture) was collected and stored at 4 °C. Before microscopy analysis, the suspension was diluted into ultrapure water (1/100), and 5 to 7 µL was deposited on copper grids coated with a lacey carbon film (porous film). The grids were air-dried for a few minutes before microscopy analysis. The analyses were performed using a transmission electron microscope (TEM), FEI Tecnai Osiris at 200 kV, coupled with an energy-dispersive X-ray spectroscopy (EDX) detection system (Super-X EDS). Imaging was conducted in bright-field (direct beam) and dark-field (annular dark field and high angular dark field; diffracted beam) mode. Chemical mapping was carried out using scanning transmission electron microscopy (STEM-EDX) and electron energy loss spectroscopy (TEM-EELS).

EDX mapping was conducted with acquisition times varying from 15 to 90 min (with an electron dose of 100 e $Å^{-2}$ s^{-1}). The chemical mapping obtained through EDX was analyzed using Esprit software (version 1.9, Bruker), and atomic proportions (at. %) were determined using the PB-ZAF algorithm. STEM-EDX mapping was conducted at scales ranging from ∼ 100 nm to a few micrometers. A total of 12 EDX mappings were carried out on the fine fractions of the forest soil, while 4 mappings were carried out on the fine fractions of the crop soil. From these mappings, various zones were selected to quantify atomic proportions, ensuring micrometric representativeness of analyzed microscopy grids (27 zones for the forest soil and 9 for the crop soil). To examine potential atomic composition heterogeneities among these zones, a principal component analysis of C, Fe, Al, and Si proportions followed by a *k*-means cluster analysis (with three imposed clusters) was performed on the selected zones using RStudio software (using the "stats", "ggplot2", and "FactoMineR" packages). Despite the lack of significant differences between the clusters, we have retained a three *k*-means clusterings (with an imposed number of clusters) to illustrate the variability in atomic composition across areas.

To ensure elemental co-localizations of C with specific elements (Al, Si, and Fe) down to a few nanometers, TEM-EELS mappings were conducted on fine fractions of both forest and crop soils. These analyses followed protocols outlined in Jamoteau et al. (2023). Briefly, the energy range examined spanned the following edges: C K-edge (284 eV), O K-edge (532 eV), Fe L-edge (708 eV), Al K-edge (1560 eV), and Si K-edge (1839 eV). To minimize beam damage while ensuring precise elemental detection at the intended scales, the analysis time per pixel was kept as short as possible. EELS data collection occurred in two phases: initially from 250 to 1224 eV with a pixel analysis duration between 0.05 to 0.09 s and subsequently from 1050 to 2074 eV with an analysis time of 0.1–1.5 s per pixel. The compilation of nanoscale-resolved elemental co-localizations was executed using a Python script available in Jamoteau et al. (2023).

2.3.2 Probing organic matter types within mineral–organic associations using STXM

To investigate the types of organic matter within mineral–organic associations, elemental maps of C, Fe, and Al, along with speciation maps of C (K-edge), were analyzed using scanning transmission X-ray microscopy (STXM) on fine fractions of forest and crop Andosols (from the 10–20 cm horizon; see part 2.2 for details on fine fraction separation). For these mappings, the fine fractions were re-humidified with ultrapure water to form a paste consistency. This mixture was instantly frozen using liquid nitrogen, and 400 nm thick sections were sliced at cryogenic temperature using a cryo-ultramicrotome (equipped with a diamond knife; Leica UC7). These sections were placed onto Si_3N_4 windows (75 nm thick, 1 × 1 mm, 100 µm; AGS172-3T, Oxford Instruments) and air-dried. STXM analyses took place at the SOLEIL synchrotron (France) on the HERMES beamline, where energy calibration was conducted for C (using CO_2 at 2 mbar) and Fe (using Fe oxides). At the edges of C, Fe, and Al, transmitted photons were recorded every 50 nm across a 5 µm × 5 µm area. The acquisition time was set to 3 ms for C- and Fe-edges and 5 ms for the Al-edge at intervals of 50 nm. The samples were first analyzed at the C K-edge with varying scan parameters: 1 eV increments between 274 and 281 eV, 0.125 eV increments between 282.125 and 292 eV, and 0.353 eV increments between 292 and 304 eV, followed by increments of 10 eV between 314 and 334 eV. Subsequently, analyses at the Fe L-edge included scan parameters of 0.5 eV increments between 700 and 705 eV, 0.15 eV increments between 705.15 and 712 eV, and finally increments of 0.5 eV between 712.5 and 730 eV. Lastly, at the Al K-edge, increments of 0.5 eV were used between 1570 and 1600 eV. Background (I_0) measurements were taken concurrently with sample analysis in an adjacent area for all edges. The C, Al, and Fe maps resulted from energy subtractions at specific intervals: C at 291.35–275 eV, Fe at 709.3–700 eV, and Al at 1588.8–1580.2 eV. Spectra from these zones were normalized using Athena software (version V0.9.26; Ravel and Newville, 2005). To assess variations in C speciation within the mappings, spectral principal component analysis of the C K-edge was performed using Orange software (version 3.35.0). However, no statistically distinct clusters were

identified in the results. Areas were then selected to illustrate the uniformity of C speciation across the maps.

3 Results

3.1 Comparison of soil physicochemical parameters between the forest and crop soils

To investigate the differences between the forest and crop soil profiles and select the appropriate horizon with quantitative differences in mineral–organic associations for microscale and nanoscale mappings, we compared key physicochemical parameters between the forest and crop Andosol profiles (Fig. 2). Results showed differences between the two soil profiles on surface horizons only, from 0 to 30 cm depth. Firstly, compared to the forest soil, the crop soil exhibited 46 % less C stock at the 0–40 cm depth, with a cumulative C difference of 66 kg C m^{-2}. Additionally, the amount of C in the fine fractions (< 20 µm, Fig. 2b), attributed to C in mineral-associated organic matter (MAOM), was lower in the crop soil compared to the forest soil, with an average of 12 and 51 gMAOM-C kg^{-1}, respectively, indicating 75 % less C in mineral–organic associations in crop topsoil. In addition, differences in pH were noticed at the 0–30 cm depth, with an averaged pH of 6.3 in the forest soil and 5.6 in the crop soil. Regarding mineralogy, both bulk and fine fractions of the forest and crop Andosols exhibited the same mineral composition including pyroxenes, orthopyroxenes, plagioclases, titanomagnetite, quartz, and gibbsite, as well as poorly crystalline phases (analyzed by XRD; see Sect. S1 in the Supplement). However, quantitative analysis of amorphous and poorly crystalline minerals, using sequential extractions with pyrophosphate and oxalate (Rennert, 2018; Rennert and Lenhardt, 2024), showed differences between the forest and crop soils. The amount of Al, Fe and Si extracted by pyrophosphate was 2 times lower in the crop soil compared to the forest soil (on the 0–20 cm depth), indicating a lower quantity of amorphous mineral phases in the crop topsoil. On the contrary, oxalate extractions did not show a clear difference between the forest and the crop soil, indicating a similar quantity of poorly crystalline minerals in both soil profiles.

In summary, the comparative analysis of soil physicochemical parameters highlighted differences between the forest and crop soil profiles (from 0–30 cm depth) by showing a lower C stock, 75 % less C in the form of mineral–organic associations, a lower abundance of amorphous mineral phases, and a variation in physicochemical parameters as indicated by a 0.7 pH disparity.

3.2 Probing types of mineral–organic associations in the forest and crop soils

3.2.1 Mineral–organic associations in the form of coprecipitates

To identify the types of mineral–organic associations in the forest and crop soils, we conducted chemical mappings using STEM-EDX (Fig. 3) on the fine fractions of the 10–20 cm horizons of both Andosols (selected for their differences in C content and physicochemical parameters; Fig. 2). These analyses confirmed previous mineralogical findings (from XRD diffractograms and sequential extractions) by identifying two distinct crystallographic phases: (1) crystalline mineral phases, ranging from a few hundred nanometers to micrometers in size, typically displaying rod-like shapes, and (2) an amorphous phase, likely in contact with the rod-like minerals (Fig. 3a and Fig. S2 for extra mappings). Across all mapped mineral–organic associations in both soils, C was invariably found within the electron amorphous phase (see Fig. 3a–b). Notably, the C was never isolated; it consistently co-occurred with a mix of Al, Si, and Fe in the electron-amorphous phase (Fig. 3c). This pattern was particularly noticeable in atomic proportions along the horizontal profile that sequentially crossed crystalline minerals (on the left side of the profile in Fig. 3d) and then amorphous phases (on the right side of the profile in Fig. 3d; see additional profiles in Sect. S2 in the Supplement), showing a marked C proportion increase upon entering and within the amorphous phase. These profiles, together with C mapping, demonstrated that C was predominantly located in the amorphous phase, closely associated with Al (∼ 20 %), Si (∼ 15 %), and to a lesser extent Fe (∼ 3 %). This nanoscale amorphous association of C with Al, Si, and Fe demonstrated that mineral–organic associations in both Andosols were formed through the coprecipitation of elements derived from mineral weathering (mainly Al, Si, and Fe) with organic matter, hereafter referred to as "coprecipitates". The interaction between coprecipitates and crystalline mineral phases may be secondary. While we cannot rule out the possibility that this interaction is induced by sample preparation (e.g., weak sonication followed by air drying), the coprecipitate–mineral interaction has been found in three different mappings and even observed between mineral sheets (Fig. S2), suggesting that such interactions may occur in soils.

3.2.2 Nanoscale structure and composition of coprecipitates

To determine the composition and nanoscale structure of the amorphous phase containing coprecipitates, we conducted high-resolution transmission electron microscopy (HRTEM) to image the coprecipitates from micrometer to nanometer scales. Figure 4 presents six images from the forest soil, representative of all the acquired images from both soils (see Sect. S3 in the Supplement for all HRTEM images).

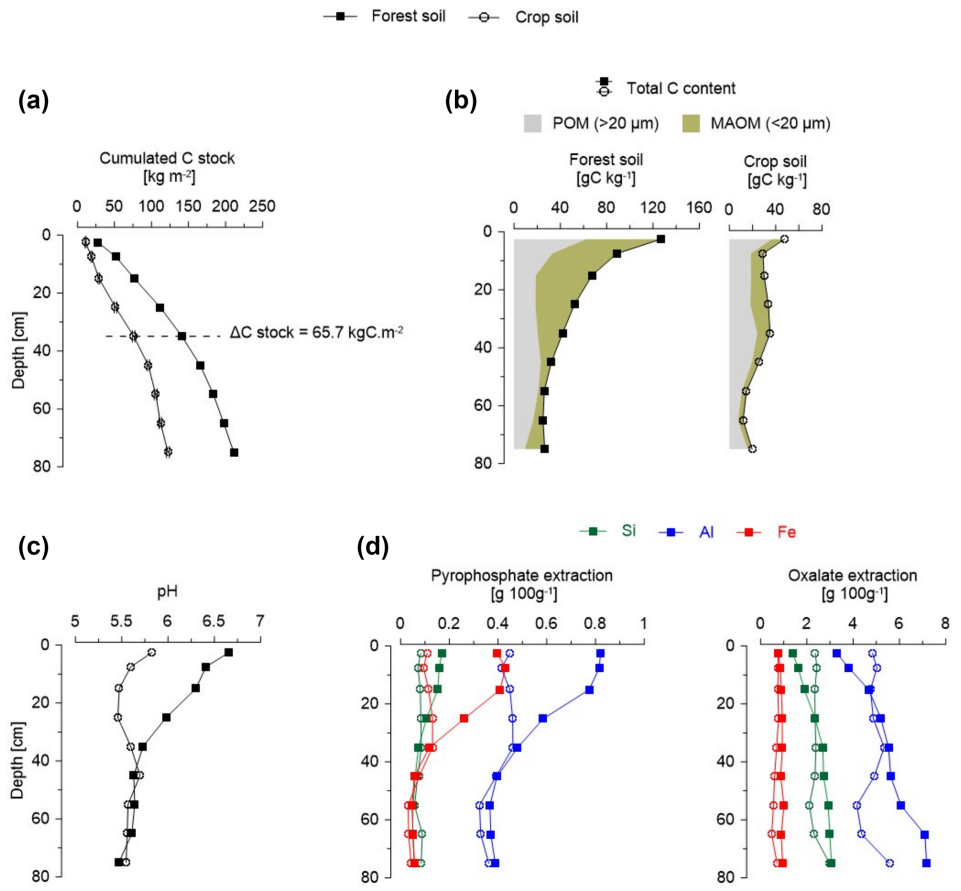

Figure 2. Soil physicochemical parameters of the forest and crop Andosols. **(a)** Cumulated C stock (corrected for equivalent mass). **(b)** Total C content and proportion of C in the form of particulate organic matter (POM) and mineral-associated organic matter (MAOM) along the soil profiles. **(c)** pH analyses along the soil profiles and **(d)** quantity of secondary mineral phases made of amorphous phases (extracted by pyrophosphate) and poorly crystalline mineral phases (extracted by oxalate).

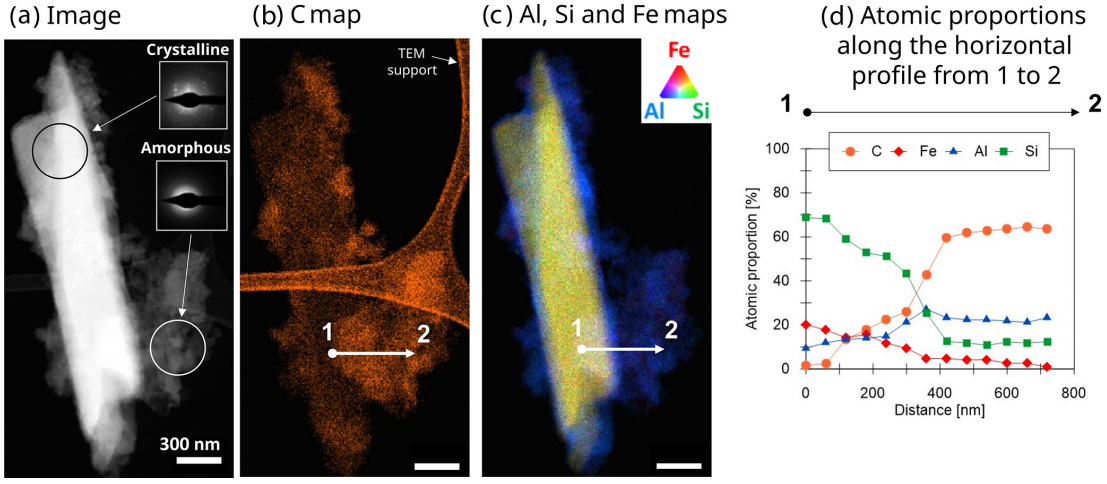

Figure 3. Chemical mapping of mineral–organic associations using STEM-EDX. This mapping was conducted on the fine fractions of the crop Andosol. For the complete set of mineral–organic association mappings, refer to Sect. S2 in the Supplement. **(a)** TEM image in dark-field mode with an electron diffraction pattern in the boxes showing the crystallinity of phases. **(b)** Carbon mapping. **(c)** Al, Si, and Fe mappings using RGB format; the white arrow indicates the location of the 700 nm horizontal profile shown in **(d)**. **(d)** Atomic proportions of C, Al, Si, and Fe along the horizontal profile.

At the micrometer to the submicrometer scale, we primarily observed aggregates and intertwined filaments (Fig. 4a–c). These filaments are indicative of imogolites, a short-range-ordered mineral forming tubular structures of Al and Si, typically resulting from ash and pumice weathering (Wada, 1985; Wada and Harward, 1974; Parfitt, 2009; Levard and Basile-Doelsch, 2016). At the nanometer scale (Fig. 4d–f), the aggregated phase primarily appeared amorphous, except for localized crystalline planes within the aggregates (as shown in Fig. 4e). The filaments have a diameter of a few nanometers (Fig. 4f), aligning with characteristics of imogolite or bundles of imogolites (Levard and Basile-Doelsch, 2016), which were very fragile under the electron beam, leading to amorphization of part of the bundles. These results were observed across numerous distinct areas (see Sect. S3 in the Supplement) in both forest and crop soils. In sum, nanoscale images demonstrated that (1) the fine fractions were predominantly composed of amorphous phases but (2) exhibited short-range-order minerals typical of imogolite (3) and showed local arrangement with some crystallinity (such as small Fe or Al oxyhydroxides), which remains very minor compared to amorphous phases.

Then, to identify elements associated with C within the amorphous phase, 12 STEM-EDX mappings were conducted on the fine fraction from the forest soil and 4 mappings on the fine fraction from the crop soil. The results, consistent across both soils, demonstrated that C was predominantly co-localized with the amorphous phase in aggregate form (Fig. 5, see Sect. S4 in the Supplement for all mappings), with minimal presence on filamentous structures associated with imogolites (indicated by arrows in Fig. 5). Further STEM-EELS mappings confirmed nanoscale co-localization of C with Al, Si, and Fe, within both forest and crop coprecipitates, below 15 nm scales (refer to Sect. S5 in the Supplement). These results indicated that the mineral component is primarily composed of a mix of amorphous Al, Si, and Fe coprecipitates, even at scales down to 15 nm, and not composed of short-range-ordered minerals like imogolite and allophane. The nanoscale co-localization of these elements (C, Al, Si, and Fe) demonstrates the presence of organic molecules coprecipitated with a mineral part such as inorganic oligomers, proto-imogolite or Fe nanophases resulting from andesite parent mineral weathering. This characterization demonstrates the wide range of coprecipitates occurring at nanoscales, such as proto-imogolite+OM, nanoCLICs, metal–organic complexes, and some Fe nanophases+OM.

3.2.3 Heterogeneity in the structure and composition of coprecipitates

After demonstrating the presence of a wide range of coprecipitate types in both soils, we further investigated the structural and chemical compositional heterogeneity between the forest and crop coprecipitates. To do this we selected various regions on coprecipitate mappings and computed the atomic proportions within the selected area of $\sim 200 \times 200$ nm (Fig. 6, see Sect. S4 in the Supplement for area localization on maps). Atomic proportions of these regions revealed comparable average compositions of coprecipitates in both forest and crop Andosols (Fig. 6a). On average, coprecipitates comprised 35 % C, 4 % N, 5 % Fe, 34 % Al, and 22 % Si. These results suggest that coprecipitates were mainly composed of organic molecules bound to an inorganic network of amorphous small oligomers up to proto-imogolites and less in the form of metal–organic complexes because, according to atomic proportions, the organic to inorganic atomic ratio $C/Al + Fe$ is 35/39, or 0.9. However, organic matter is in the form of molecules containing a minimum of 8 to 10 C atoms, with 2 to 3 reactive sites per molecule able to bind to inorganic elements (by covalent or weak bonds). Then, if 3 reactive sites are present for 10 C atoms, the ratio of reactive sites to inorganic atoms ($R/Al + Fe$) is 0.3. Moreover, Si (not taken into account in this calculation) also competes with the reactive sites of Al and Fe (Lenhardt et al., 2023). According to the atomic proportions acquired, it is impossible for all organic matter to be bound to only a single Al or Fe monomer in the form of metal–organic complexes. Hence, most organic molecules must be predominantly bound to oligomers (2–3 inorganic atoms made of Al, Fe, and Si) in the form of nanoCLICs and proto-imogolites. Moreover, these averaged proportions masked underlying heterogeneities in atomic proportion within coprecipitates, including areas with high C+Al+Si proportions (averaging 44 % C, 6 % N, 2 % Fe, 32 % Al, and 17 % Si), areas with high C+Fe+Al+Si proportions (44 % C, 5 % N, 14 % Fe, 23 % Al, and 13 % Si), and areas with high Al+Si proportions but lower C proportions (21 % C, 3 % N, 2 % Fe, 42 % Al, and 32 % Si; see Fig. 4e). Such heterogeneities were noted in both the forest and crop coprecipitates (Fig. 6b), indicating a consistent variation in elemental proportions within the coprecipitates. Following the same logic as above, C+Al+Si-rich and Al+Si-rich zones (with less C) can be attributed to zones containing mainly coprecipitates in the form of C+Al+Si nanoCLICs and proto-imogolite+OM. Concerning the C+Fe+Al+Si-rich zones, additional coprecipitate forms may be present, such as C+Fe+Al+Si nanoCLICs and some Fe nanophases associated with organic matter. Therefore, all these forms of coprecipitate can be categorized as amorphous coprecipitates.

Subsequently, to determine whether the nature of organic matter could affect these heterogeneities (i.e., selective associations with an elemental mix of Al, Si, and Fe), we conducted elemental mapping for C, Al, and Fe using scanning transmission X-ray microscopy (STXM; see Fig. 7a) and assessed the elemental speciation of carbon through C K-edge analyses (Fig. 7b). The elemental mappings for C, Al, and Fe corroborated the findings from STEM-EDX and STEM-EELS analyses: specifically, a dominant co-localization of C with Al (as indicated by purple in Fig. 7a), with heterogeneities in regions of a few hundred nanometers ($\sim 500 \times$

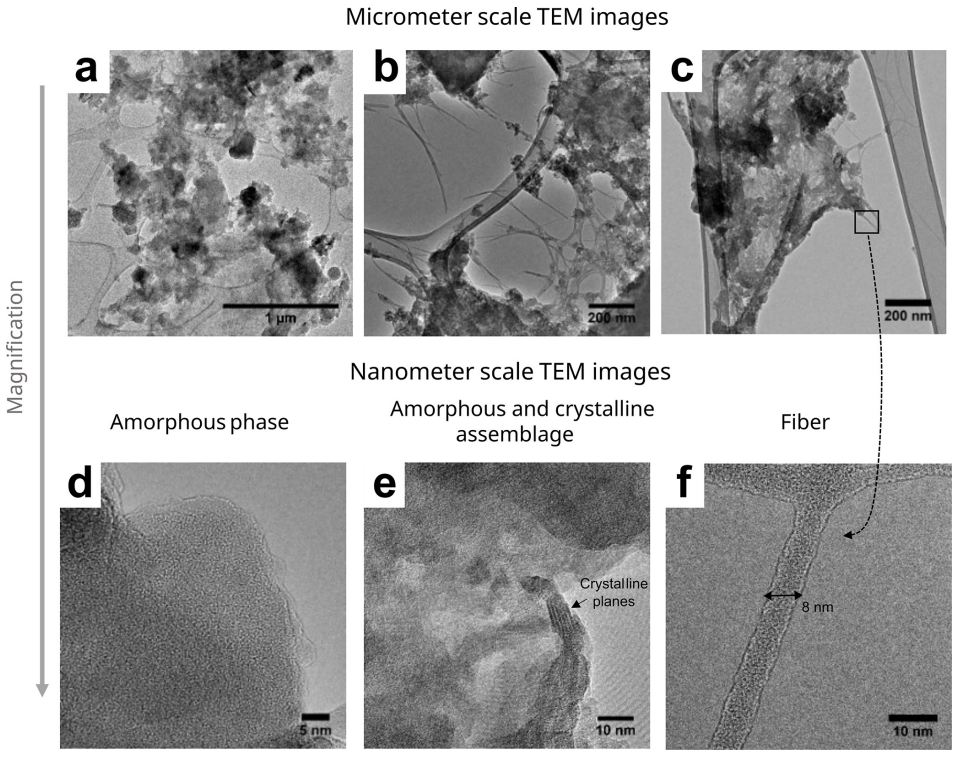

Figure 4. High-resolution TEM analysis of the amorphous aggregated phase and filaments. Microscale **(a–c)** and nanoscale **(d–f)** images of the amorphous aggregated phase and filaments. **(d)** Nanoscale image of the amorphous aggregated phase. **(e)** Localized crystallization within the aggregates (see crystalline planes). **(f)** Nanoscale image of an ∼ 8 nm diameter filament, characteristic of imogolite minerals. The sample holder is denoted by white arrows. These images were acquired on the fine fraction of the forest soil; for additional images in both soils, refer to Sect. S3 in the Supplement.

500 nm), locally enriched in Fe (see areas 6, 7, and 8 in Fig. 7a), Al (area 5), or C (areas 3 and 4) observed in both the forest and crop soils. Overall, C speciation results exhibited multiple peaks indicative of aromatic C (∼ 285 eV), phenolic C and ketonic C (∼ 286.6 eV), carboxylic C (∼ 288.4 eV), and carbonyl C (∼ 290.4 eV; Francis and Hitchcock, 1992; Cody et al., 1998; Boyce et al., 2002; Wan et al., 2007; Cosmidis and Benzerara, 2014; Le Guillou et al., 2018). Cluster analysis of the C K-edge did not reveal any distinct zones with different C speciation (see Sect. S6 in the Supplement), nor did it indicate any differences in C speciation between the forest and crop coprecipitates. Within the localized enriched area, a similar diversity of organic matter was detected in areas richer in C+Al+Fe (areas 1, 2, 8, 9), areas richer in C+Fe (areas 6, 7, 10), and areas richer in C+Al (area 5). Only the area enriched in C displayed distinct speciation, predominantly consisting of aromatic C (∼ 285 eV) and carboxylic C (∼ 288.4 eV). Moreover, compared to the area enriched in C, the speciation of C within coprecipitates richer in C+Al+Fe and C+Fe showed a higher peak at 286.6 eV attributed to organic compounds made of phenolic C and ketonic C. These results indicated that a broad spectrum of organic molecules is present within amorphous coprecipitates of the forest and crop soils.

4 Discussion

4.1 Mineral–organic associations in Andosols: a diversity of amorphous coprecipitates

Mineral–organic associations are typically conceptualized as organic matter adsorbed or coprecipitated with secondary minerals (Kleber et al., 2015, 2021). In Andosols, these associations are conceptualized as organic matter adsorbed on short-range-ordered minerals such as imogolite, allophane, and ferrihydrite (Wada and Harward, 1974; Wada, 1985; Kleber et al., 2004; Parfitt, 2009). However, certain Andosols have been shown to lack these short-range-ordered minerals (Levard et al., 2012), and nanoscale analyses revealed the presence of mineral–organic associations in the form of nanoCLICs (nanosized coprecipitates of inorganic oligomers with organics), proto-imogolite+OM, and some Fe nanophases+OM and metal–organic complexes (this study and in Jamoteau et al., 2023). More surprisingly, in this study, some short-range-order minerals in the form of imogolite were observed; however, most of the C was in amorphous coprecipitates made of nanoCLICs, proto-imogolite+OM, some Fe nanophases+OM, and some metal–organic complexes. These mixes of coprecipitates are more amorphous

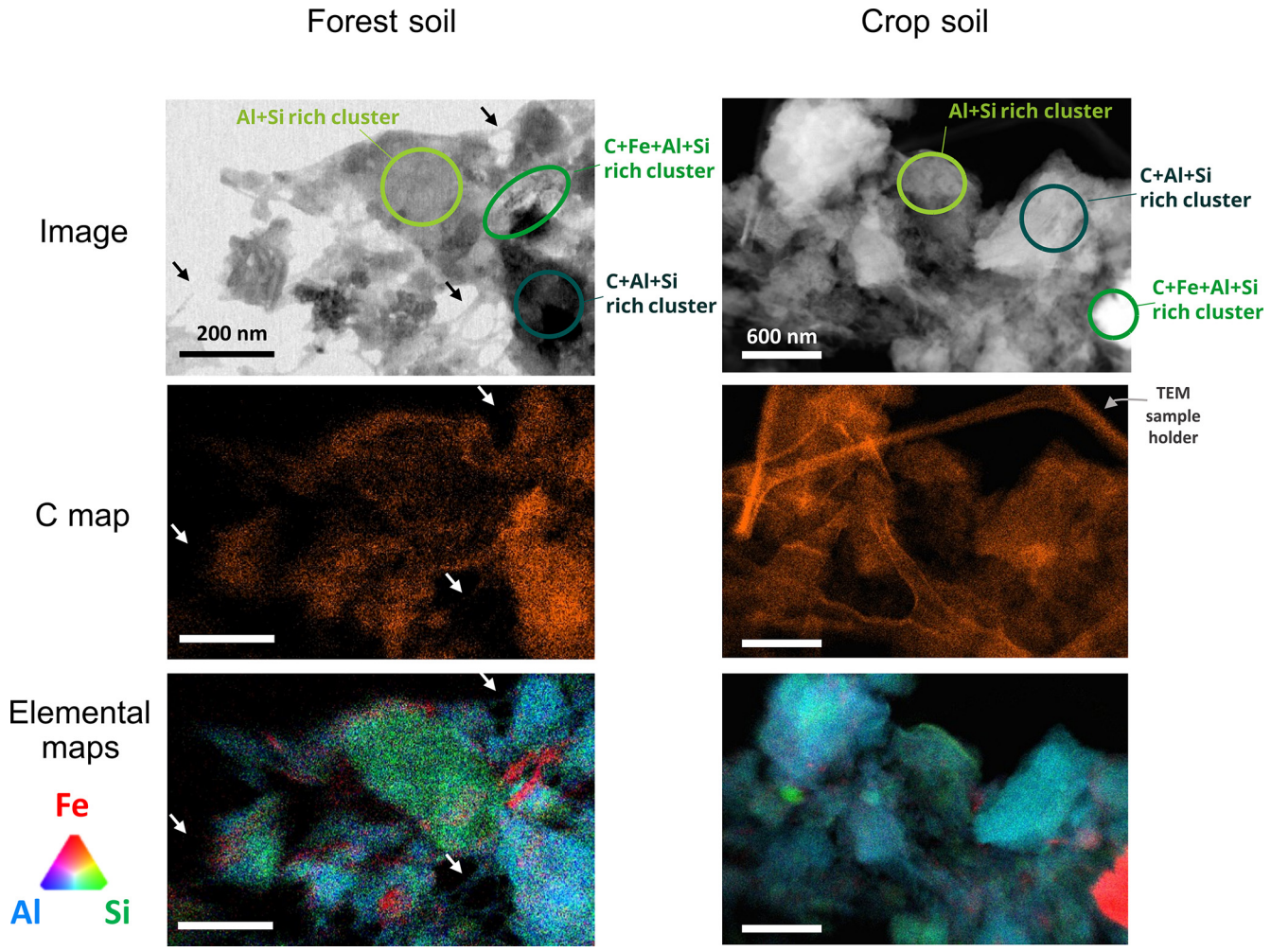

Figure 5. Chemical mapping of forest and crop coprecipitates using STEM-EDX. Chemical mapping of coprecipitates from the forest and the crop soil, showing imaged areas, carbon detections, and detections of Al, Si and Fe. Arrows indicate fibers characteristic of imogolites. See Sect. S4 in the Supplement for additional mappings of forest and crop soils. The circled areas feature zones richer in C+Al+Si, C+Fe+Al+Si, and Al+Si (with less C).

and heterogeneous than previously proposed models of minerals in mineral–organic associations, with their amorphous nature likely preserved by Si and organic matter that inhibit crystallization of short-range-ordered minerals (Levard et al., 2012; Lenhardt et al., 2022, 2023). Mineral–organic association in the form of amorphous coprecipitates are thus found in different Andosols: in an Andosol formed a few hundred years ago on andesite parent material (Fe-poor parent material, this study) and in an Andosol formed 40 000 years ago on basalt parent material (Fe-rich parent material, Jamoteau et al., 2023). Such amorphous mineral forms are likely present in many other Andosols, particularly young Andosols (e.g., Shimada et al., 2022). These Andosols showed strong correlations between C and pyrophosphate-extractable metals (Alpp + Fepp), which primarily extracts metals from the least polymerized phases. However, before generalizing mineral–organic associations in the form of amorphous coprecipitates to all Andosols, future analyses must examine a broader range of Andosol types, considering various parent materials, ages, and climates.

4.2 Heterogeneous chemical composition of amorphous coprecipitates

In these amorphous coprecipitates, our results showed an amorphous elemental mixture of C, Al, Si, and Fe. However, the proportions of these elemental mixtures showed enrichments in Al, Si, and Fe, with varying amounts of C, down to the scale of 100 nm (see Fig. 8a), likely forming C+Al+Si and C+Fe+Al+Si nanoCLICs, proto-imogolite+OM, some Fe nanophase+OM, and metal–organic complexes. However, we propose that these phases should not be conceptualized as distinct entities. Instead, a continuum of phases should be considered, as illustrated by the ternary diagram

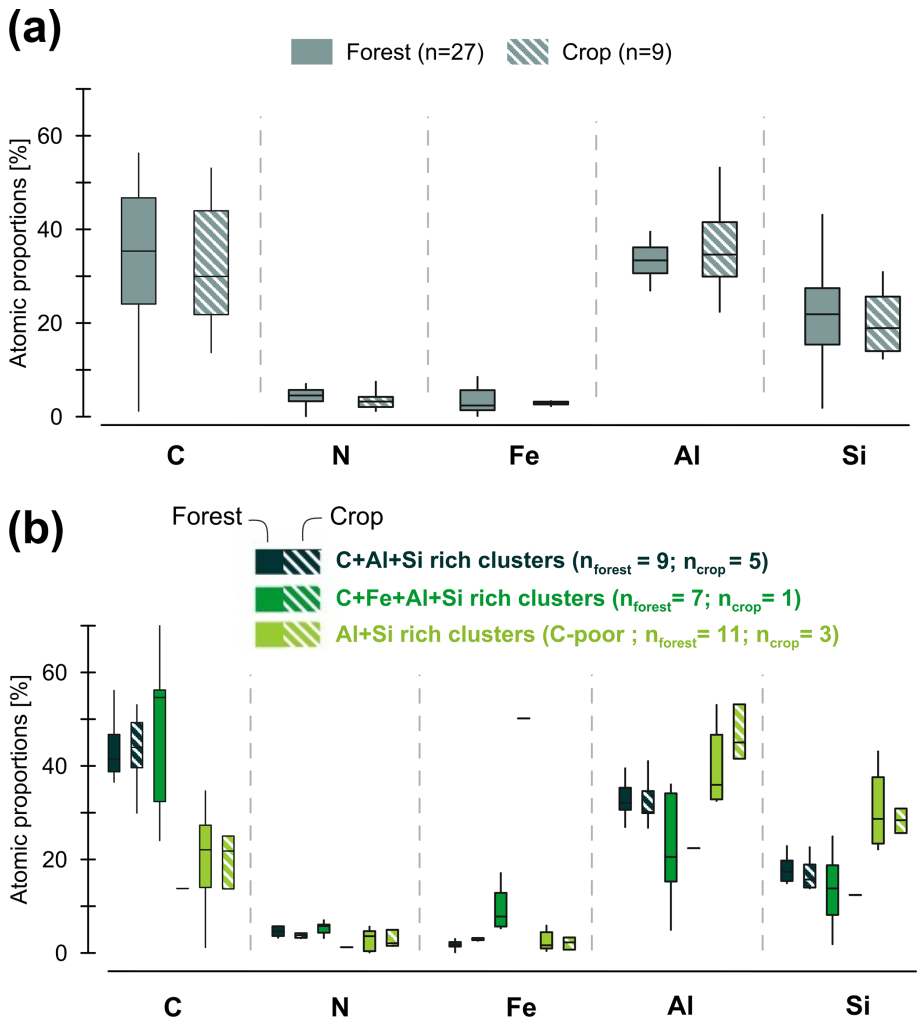

Figure 6. Atomic composition of forest and crop coprecipitates based on STEM-EDX mapping. From STEM-EDX mapping, various regions were selected to compute atomic proportions within the selected area of $\sim 200 \times 200$ nm. **(a)** The average atomic proportions from selected areas across all mappings conducted for forest and crop soil coprecipitates, with *n* representing the number of areas averaged. **(b)** Cluster-specific atomic proportions for clusters rich in C+Al+Si, C+Fe+Al+Si, and Al+Si (C poor) across various selected areas from all mappings of forest and crop soil coprecipitates. *n* denotes the number of areas averaged. Examples of selected areas categorized as C+Al+Si, C+Fe+Al+Si, and Al+Si (C-poor) are shown in Fig. 5.

in Fig. 8b. This diagram shows distinct entities comprising (1) nanoCLICs enriched in C+Fe+Al+Si, (2) nanoCLICs enriched in C+Al+Si and proto-imogolites+OM, and (3) nanoCLICs enriched in C+Si+Al (Si rich) along with their intermediate forms. In addition to these predominant forms, the small amount of Fe in coprecipitates could also be present in the form of (4) Fe nanophases+OM and (5) metal–organic complexes. This compositional heterogeneity in the mineral (or inorganic) portion of the coprecipitates may arise from their formation in microsites with locally diverse elemental solutions. For instance, this could be influenced by the proximity to certain minerals that release specific elements into the soil solution, a process potentially controlled by microbial activity (Uroz et al., 2009; Bonneville et al., 2011, 2016). An alternative hypothesis for the compositional heterogeneity relates to the nature of organic matter, which might bind preferentially to certain elemental mixtures of Al, Si, and Fe. Our findings demonstrate that overall, the organic matter speciation was diverse (composed of aromatic C, phenolic C, ketonic C, carboxylic C, and carbonyl C) and consistent across areas down to the scale of 100 nm (Fig. 7). This finding aligns well with the diversity of organic matter observed in mineral–organic associations from various temperate and tropical soils, despite distinct vegetation compositions and soil mineralogy (Kinyangi et al., 2006; Lehmann et al., 2008; Solomon et al., 2012; Asano et al., 2018), and demonstrates that a broad spectrum of organic matter can form mineral–organic associations in the form of amorphous coprecipitates. However, in areas richer in C+Al+Fe and C+Fe, a higher proportion of organic com-

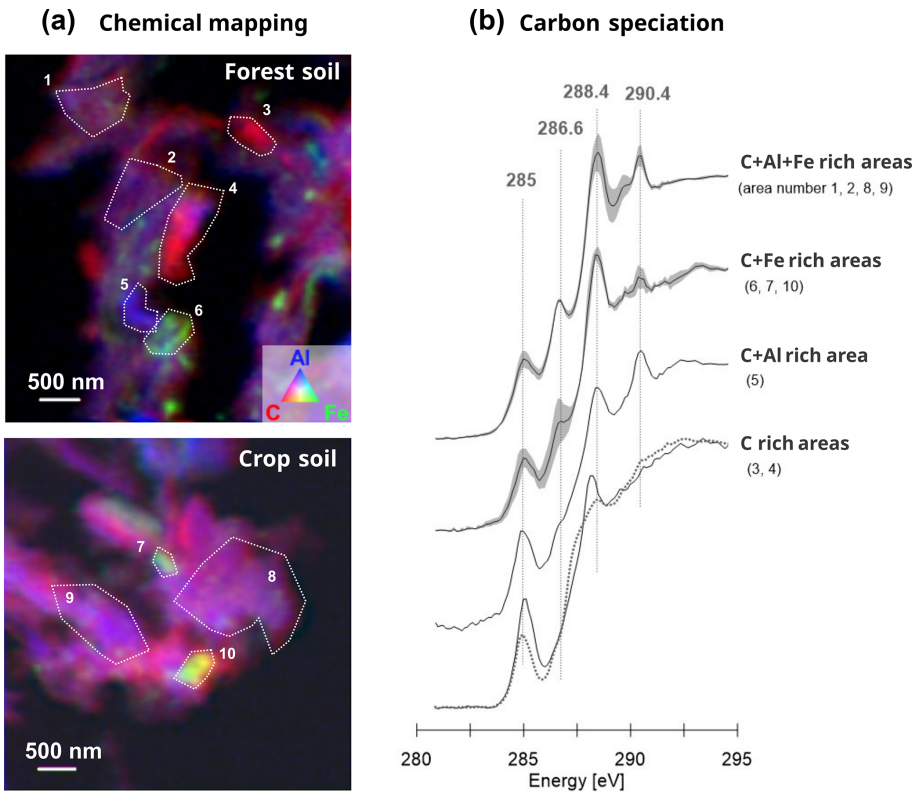

Figure 7. Chemical mapping and organic matter characterization in coprecipitates using STXM mapping. **(a)** STXM chemical mappings at the C K-edge, Fe L-edge, and Al K-edge of coprecipitates from forest and crop soils. **(b)** C K-edge spectra of the delineated area (outlined in panel **a**) showing the principal energy bands associated with aromatic C (~ 285 eV), phenolic C and ketonic C (~ 286.6 eV), carboxylic C and C–OH (~ 288.4 eV), and carbonyl C (~ 290.4 eV). C speciation exhibited consistency across the coprecipitates of both forest and crop soils (see individual spectra in Sect. S6 in the Supplement).

pounds made of phenolic C and ketonic C were observed (Fig. 7), suggesting a correlation between the presence of Fe in coprecipitates and phenolic and/or ketonic-rich compounds. This correlation could be explained by a preferential binding of phenolic compounds with Fe, highlighted in the literature (Schmidt et al., 2013; Mimmo et al., 2014). Moreover, the enrichment in aromatic C in C-rich areas (not associated with other elements) aligns with findings in other soil types (Solomon et al., 2012; Lutfalla et al., 2019) and may stem from the presence of particulate organic matter, thus indicating more degraded organic matter in coprecipitates. In conclusion, these results highlight the complex and heterogeneous nature of amorphous coprecipitates in Andosols. These findings underscore the importance of considering a continuum of coprecipitate phases rather than distinct entities to better understand the interactions between organic matter and amorphous mineral components in soils.

4.3 A secondary interaction: adsorption of amorphous coprecipitates onto mineral surfaces

In prevailing conceptual frameworks of mineral–organic associations, two dominant paradigms are recognized: coprecipitation and adsorption of organic matter with minerals (Kleber et al., 2015, 2021). Our investigations reveal that amorphous coprecipitates represent the main form of mineral–organic associations in some Andosols. However, a secondary association was observed: adsorption of amorphous coprecipitates onto mineral surfaces (Figs. 3 and 8) or within phyllosilicate layers (refer to Sect. S2 in the Supplement) and likely adsorption onto short-range-order surfaces (e.g., imogolite, Fig. 5). These findings suggest that coprecipitation processes likely occur either upstream or simultaneously with adsorption processes on mineral surfaces. These processes can take place in soil solutions, which contain both organic compounds and elements resulting from mineral weathering (such as Si, Al, Fe, Ca, and Mn; Campbell et al., 1989; Giesler and Lundström, 1993; Manderscheid and Matzner, 1995; Strobel et al., 2001; Kaiser et al., 2002). Coprecipitation and subsequent adsorption on mineral surfaces are, therefore, interrelated phenomena. This study highlights that mineral–organic associations need to be conceptualized as a sum of subsequent interactions rather than a single interaction (as amorphous coprecipitates being adsorbed onto mineral surfaces), thereby illustrating the complexity of mineral–organic association assemblages in soils. More-

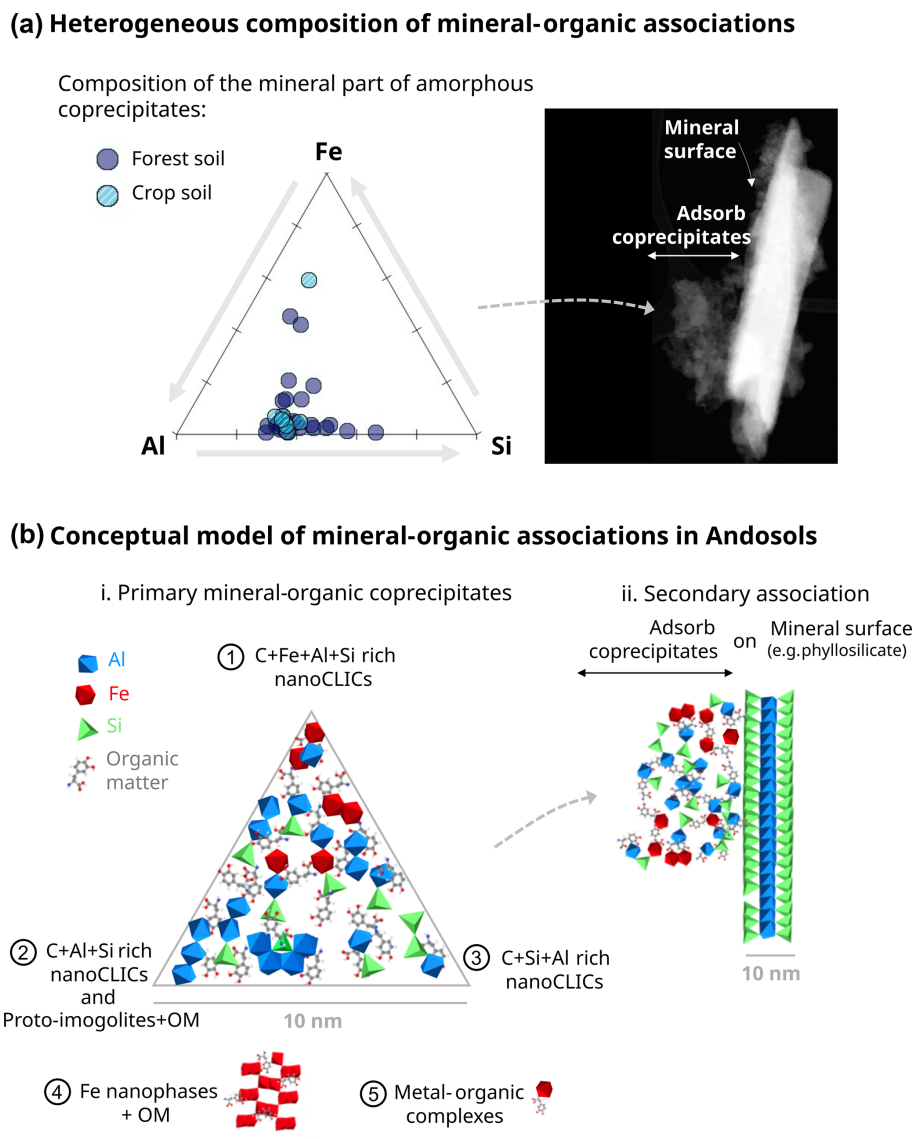

Figure 8. Structure and composition of mineral–organic associations in Andosols. **(a)** Atomic proportions of Al, Si, and Fe in mineral–organic associations in the amorphous phase derived from STEM-EDX mappings. The right panel image illustrates the type of area analyzed by STEM-EDX, highlighting regions where amorphous coprecipitates have been found adsorb on a crystal's surfaces. **(b)** Conceptual model of primary mineral–organic associations in Andosols. (i) Primary mineral–organic coprecipitates comprising a mix of nanoCLICs, proto-imogolites+OM (numbers 1, 2, and 3), Fe nanophases+OM (4), and metal–organic complexes (5). The ternary diagram depicts the compositional heterogeneity of these amorphous coprecipitates and the continuum of forms between C+Fe+Al+Si-rich nanoCLICs (1), C+Al+Si-rich nanoCLICs, and proto-imogolites (2) and C+Si+Al-rich nanoCLICs (3). Additionally, a conceptual model of secondary association is presented, showcasing the interaction of primary mineral–organic coprecipitates with mineral surfaces (e.g., 2 : 1 phyllosilicate).

over, this secondary association between coprecipitates and mineral surfaces aligns with studies demonstrating the binding capacity of mineral–organic associations in Andosols (Wagai et al., 2018; Asano et al., 2018; Shimada et al., 2022). This binding capacity between amorphous mineral–organic association and fine soil minerals could contribute to the structuration of aggregates, particularly clay-sized aggregates (Asano et al., 2018; Wagai et al., 2018; Shimada et al., 2022). In sum, our results underscore the complexity of primary and secondary mineral–organic associations in soils, highlighting the interplay between coprecipitation and adsorption processes. These interactions are crucial for soil organic matter stabilization and the formation and stability of soil aggregates.

4.4 Differences between the forest and crop soils: toward a quantitative loss of amorphous coprecipitates rather than changes in mineral–organic association types

The transition from natural to agricultural systems typically results in a C stock decline (Poeplau and Don, 2013; Sanderman et al., 2017). In the studied Andosols, the crop soil had 46 % less C stock compared to the forest soil at 0–30 cm depth (Fig. 2), consistent with previous findings following forest-to-crop conversions in the literature (Poeplau and Don, 2013). This substantial C difference showed up to 75 % less C in mineral–organic association in the crop topsoil compared to the forest topsoil. However, the same types of mineral–organic associations were present in both Andosols: nanoscale examination exhibits amorphous coprecipitates characterized by similar inorganic structural heterogeneity and organic matter diversity (Figs. 5–7). Moreover, pyrophosphate extractions on bulk soils highlighted a twofold difference in the extracted amount of Al, Si, and Fe between the forest on the crop Andosols, suggestive of fewer amorphous mineral phases in the crop soil (Rennert, 2018; Rennert and Lenhardt, 2024). These extractions should specifically target the amorphous coprecipitates and imogolites observed at the nanoscale (Fig. 4) in this context. Compared to the forest topsoil, the lower amount of C within mineral–organic associations simultaneous to the lower quantity of amorphous and poorly crystalline minerals in the crop topsoil suggests a lower abundance of amorphous coprecipitates in the crop topsoil. Furthermore, although the total C content in the crop topsoil was lower, the relative C proportion within the amorphous coprecipitates remained similar to the ones in the forest topsoil (Fig. 6, within the limits of the analyzed areas), further indicating fewer amorphous coprecipitates in the crop topsoil (and not only a lower C content within the amorphous coprecipitates). Ultimately, these results suggest that the cropland conditions mainly affected the quantity, rather than the type, of mineral–organic associations in the studied Andosol. However, it is important to consider that the representativeness of a forest-to-cropland conversion in this study has some limitations: firstly, the samples come from only one soil profile taken at a single point in time, which means they may not fully capture the spatial variability within a plot. Secondly, the quantitative differences in organic carbon content and extractable pools are based on a single observation per depth. Although multiple depths within a profile contribute valuable information to the overall pattern, they do not function as replicates per se.

4.5 Insights into the stability of mineral–organic associations in Andosols

In the literature, mineral–organic associations are considered to be stable over centennial durations (Trumbore et al., 1989; Bol et al., 2009; Feng et al., 2016; Shimada et al., 2022). However, in Andosols, which are rich in mineral–organic associations, just a few decades of cultivation can lead to the destabilization of C (Verde et al., 2005; Basile-Doelsch et al., 2009; Osher et al., 2003; Dube et al., 2009; Koga et al., 2020). In this study, if the two analyzed Andosol profiles represent decreases between forest and crop soil (see the limits of sample representativeness of forest-to-cropland conversion in Sect. 4.4), our results suggest that (i) the observed difference in C content can be primarily due to the disruption of mineral–organic associations within the 0–30 cm depth of the Andosol, and (ii) mineral–organic associations in the form of amorphous coprecipitates may be prone to destabilization after 3 decades of agricultural activity. This indicates that while such associations may persist for a long time within certain Andosols, they can be susceptible to disruption contingent upon agricultural practices. This potential disruption could be linked to the disruption of amorphous mineral constituents of coprecipitates, namely Al, Si, and Fe – given that amorphous Al and Fe exhibit diminished stability under reduced pH conditions. Consequently, amorphous coprecipitates may experience partial solubilization as a result of the pH diminution in the crop soil, potentially leading to the loss of these associations. Despite a total pH difference of approximately 1 unit, from 6.3 in the forest soil to 5.6 in the crop soil (Fig. 2), this overall lower pH in the crop soil could reflect even lower pH driven by root exudates and the biological activity (Keiluweit et al., 2015; Bernard et al., 2022), potentially leading to coprecipitate disruption. Moreover, given the heterogeneous composition of amorphous coprecipitates (Fig. 8), their transformations could have varied based on local composition. For example, amorphous coprecipitates with a high Fe content may exhibit increased sensitivity to redox fluctuations and pH decreases, while those enriched with Al and Si may show sensitivity to pH changes. Such compositional-dependent transformations were not found in our results, which demonstrated consistent heterogeneity of amorphous coprecipitates across both forest and crop Andosols (Fig. 4). In addition to their chemical vulnerability to physicochemical changes, agricultural activity may also play a role in amorphous coprecipitates disruption by lessening aggregate occlusion, enhancing interaction between the microbial community, roots, and coprecipitates (Bailey et al., 2019). Consequently, if the two analyzed Andosol profiles represent decreases in mineral–organic associations between the forest and crop soils, this study would suggest that mineral–organic associations in the form of amorphous coprecipitates could be prone to disruption due to agricultural conversion.

5 Conclusions

The investigation of mineral–organic association types down to the microscale and nanoscale in the studied Andosol demonstrated the presence of amorphous coprecipitates,

made of a mix of nanoCLICs, proto-imogolite+OM and some Fe nanophases+OM, and metal–organic complexes. These amorphous coprecipitates observed in both the forest and crop soils exhibited the same amorphous composition and chemical heterogeneity, challenging prior conceptualization of mineral–organic associations in Andosols by demonstrating the presence of amorphous coprecipitates rather than solely organic matter associated with short-range-order minerals, such as imogolite and allophanes. The organic matter composition of amorphous coprecipitates was diverse, made of aromatic C, phenolic C, ketonic C, carboxylic C, and carbonyl C, suggesting the potential for coprecipitate formation with various types of organic matter. Moreover, our spatial mapping suggests that these amorphous coprecipitates can adhere to mineral surfaces (i.e., onto phyllosilicates and imogolites), suggesting that such associations are a composite of multiple interactions rather than a singular form. These results underscore the complexity of primary mineral–organic associations and their subsequent interactions in soils, highlighting the interplay between coprecipitation and adsorption processes. These interactions are crucial for soil organic matter stabilization and the formation and stability of soil aggregates, particularly at the clay size level. While the crop topsoil was observed to have 75 % less C in mineral–organic associations than the forest topsoil, alongside notable physicochemical differences, including a lower pH, the presence of similar amorphous coprecipitates in both forest and crop soils was confirmed. Although the sample size for comparing land use types is limited, the findings suggest that land use differences did not significantly influence the nature of mineral–organic associations or the C content within the amorphous coprecipitates but rather suggest an effect on the quantity of amorphous coprecipitates in the crop topsoil. This study demonstrates the crucial role of amorphous coprecipitates in C stabilization in Andosols but also suggests their vulnerability to disruption after 30 years of agricultural conversion, thereby challenging our understanding of the persistence of mineral–organic associations in Andosols.

Data availability. Data are available upon request from the corresponding author.

Supplement. The supplement related to this article is available online at https://doi.org/10.5194/soil-11-535-2025-supplement.

Author contributions. FJ contributed to conceptualization, methodology, formal analysis, and writing (original draft). ED participated in conceptualization, methodology, formal analysis, and writing (review and editing). NC and CL were involved in conceptualization, methodology, formal analysis, and writing (review and editing). TW, FSA, SuS, AD, DB, MLP, PC, VV, and NB contributed to sampling, methodology, and formal analysis. IDB participated in conceptualization, methodology, formal analysis, and writing (review and editing).

Competing interests. The contact author has declared that none of the authors has any competing interests.

Disclaimer. Publisher's note: Copernicus Publications remains neutral with regard to jurisdictional claims made in the text, published maps, institutional affiliations, or any other geographical representation in this paper. While Copernicus Publications makes every effort to include appropriate place names, the final responsibility lies with the authors.

Acknowledgements. The authors thank Stefan Stanescu for his support during analyses on the HERMES beamline at the SOLEIL synchrotron and Marco Keiluweit for his edits to the paper. The authors thank the PiCSL-FBI core platform (IBDM, AMU-Marseille, member of the France-BioImaging national research infrastructure, ANR-10-INBS-04), where the cryo-sections were conducted. We thank the anonymous reviewers for their constructive and insightful comments, which greatly contributed to improving this paper.

Financial support. This research has been supported by the Agence Nationale de la Recherche (grant nos. ANR-16-CE01-0012-02 and ANR-10-INBS-04), the Equipex nanoID platform (2010–2019), and la Région SUD and CIRAD (Emploi Jeunes Doctorants, subvention no. 2019_03559, DEB 19-574).

Review statement. This paper was edited by Jocelyn Lavallee and reviewed by two anonymous referees.

References

Asano, M., Wagai, R., Yamaguchi, N., Takeichi, Y., Maeda, M., Suga, H., and Takahashi, Y.: In Search of a Binding Agent: Nano-Scale Evidence of Preferential Carbon Associations with Poorly-Crystalline Mineral Phases in Physically-Stable, Clay-Sized Aggregates, Soil Syst., 2, 32, https://doi.org/10.3390/soilsystems2020032, 2018.

Bailey, V. L., Pries, C. H., and Lajtha, K.: What do we know about soil carbon destabilization?, Environ. Res. Lett., 14, 083004, https://doi.org/10.1088/1748-9326/ab2c11, 2019.

Basile-Doelsch, I., Brun, T., Borschneck, D., Masion, A., Marol, C., and Balesdent, J.: Effect of landuse on organic matter stabilized in organomineral complexes: A study combining density fractionation, mineralogy and δ^{13}C, Geoderma, 151, 77–86, https://doi.org/10.1016/j.geoderma.2009.03.008, 2009.

Basile-Doelsch, I., Balesdent, J., and Rose, J.: Are Interactions between Organic Compounds and Nanoscale Weathering Minerals the Key Drivers of Carbon Storage in Soils?, Environ. Sci. Technol., 49, 3997–3998, https://doi.org/10.1021/acs.est.5b00650, 2015.

Basile-Doelsch, I., Balesdent, J., and Pellerin, S.: Reviews and syntheses: The mechanisms underlying carbon storage in soil, Biogeosciences, 17, 5223–5242, https://doi.org/10.5194/bg-17-5223-2020, 2020.

Bernard, L., Basile-Doelsch, I., Derrien, D., Fanin, N., Fontaine, S., Guenet, B., Karimi, B., Marsden, C., and Maron, P.-A.: Advancing the mechanistic understanding of the priming effect on soil organic matter mineralisation, Funct. Ecol., 36, 1355-77, https://doi.org/10.1111/1365-2435.140, 2022.

Bol, R., Poirier, N., Balesdent, J., and Gleixner, G.: Molecular turnover time of soil organic matter in particle-size fractions of an arable soil, Rapid Commun. Mass Spectrom., 23, 2551–2558, https://doi.org/10.1002/rcm.4124, 2009.

Bonneville, S., Morgan, D. J., Schmalenberger, A., Bray, A., Brown, A., Banwart, S. A., and Benning, L. G.: Tree-mycorrhiza symbiosis accelerate mineral weathering: Evidences from nanometer-scale elemental fluxes at the hypha–mineral interface, Geochim. Cosmochim. Ac., 75, 6988–7005, https://doi.org/10.1016/j.gca.2011.08.041, 2011.

Bonneville, S., Bray, A. W., and Benning, L. G.: Structural Fe(II) Oxidation in Biotite by an Ectomycorrhizal Fungi Drives Mechanical Forcing, Environ. Sci. Technol., 50, 5589–5596, https://doi.org/10.1021/acs.est.5b06178, 2016.

Boyce, C. K., Cody, G. D., Feser, M., Jacobsen, C., Knoll, A. H., and Wirick, S.: Organic chemical differentiation within fossil plant cell walls detected with X-ray spectromicroscopy, Geology, 30, 1039–1042, https://doi.org/10.1130/0091-7613(2002)030<1039:OCDWFP>2.0.CO;2, 2002.

Campbell, D. J., Kinniburgh, D. G., and Beckett, P. H. T.: The soil solution chemistry of some Oxfordshire soils: temporal and spatial variability, J. Soil Sci., 40, 321–339, https://doi.org/10.1111/j.1365-2389.1989.tb01277.x, 1989.

Chen, C., Dynes, J. J., Wang, J., and Sparks, D. L.: Properties of Fe-organic matter associations via coprecipitation versus adsorption, Environ. Sci. Technol., 48, 13751–13759, https://doi.org/10.1021/es503669u, 2014.

Cody, G. D., Ade, H., Wirick, S., Mitchell, G. D., and Davis, A.: Determination of chemical-structural changes in vitrinite accompanying luminescence alteration using C-NEXAFS analysis, Org. Geochem., 28, 441–455, https://doi.org/10.1016/S0146-6380(98)00010-2, 1998.

Cosmidis, J. and Benzerara, K.: Soft x-ray scanning transmission spectromicroscopy, in: Biomineralization Sourcebook, CRC Press, https://doi.org/10.1201/b16621, 2014.

Cotrufo, M. F., Ranalli, M. G., Haddix, M. L., Six, J., and Lugato, E.: Soil carbon storage informed by particulate and mineral-associated organic matter, Nat. Geosci., 12, 989–994, https://doi.org/10.1038/s41561-019-0484-6, 2019.

Derrien, D., Barré, P., Basile-Doelsch, I., Cécillon, L., Chabbi, A., Crème, A., Fontaine, S., Henneron, L., Janot, N., Lashermes, G., Quénéa, K., Rees, F., and Dignac, M.-F.: Current controversies on mechanisms controlling soil carbon storage: implications for interactions with practitioners and policy-makers. A review, Agron. Sustain. Dev., 43, 21, https://doi.org/10.1007/s13593-023-00876-x, 2023.

Dube, F., Zagal, E., Stolpe, N., and Espinosa, M.: The influence of land-use change on the organic carbon distribution and microbial respiration in a volcanic soil of the Chilean Patagonia, Forest Ecol. Manag., 257, 1695–1704, 2009.

Ellert, B. H. and Bettany, J. R.: Calculation of organic matter and nutrients stored in soils under contrasting management regimes, Can. J. Soil Sci., 75, 529–538, https://doi.org/10.4141/cjss95-075, 1995.

Even, R. J. and Cotrufo, M. F.: The ability of soils to aggregate, more than the state of aggregation, promotes protected soil organic matter formation, Geoderma, 442, 116760, https://doi.org/10.1016/j.geoderma.2023.116760, 2024.

Feng, W., Shi, Z., Jiang, J., Xia, J., Liang, J., Zhou, J., and Luo, Y.: Methodological uncertainty in estimating carbon turnover times of soil fractions, Soil Biol. Biochem., 100, 118–124, https://doi.org/10.1016/j.soilbio.2016.06.003, 2016.

Fontaine, S., Abbadie, L., Aubert, M., Barot, S., Bloor, J. M. G., Derrien, D., Duchene, O., Gross, N., Henneron, L., Le Roux, X., Loeuille, N., Michel, J., Recous, S., Wipf, D., and Alvarez, G.: Plant–soil synchrony in nutrient cycles: Learning from ecosystems to design sustainable agrosystems, Glob. Change Biol., 30, e17034, https://doi.org/10.1111/gcb.17034, 2024.

Francis, J. T. and Hitchcock, A. P.: Inner-shell spectroscopy of p-benzoquinone, hydroquinone, and phenol: distinguishing quinoid and benzenoid structures, J. Phys. Chem., 96, 6598–6610, https://doi.org/10.1021/j100195a018, 1992.

Giesler, R. and Lundström, U.: Soil Solution Chemistry: Effects of Bulking Soil Samples, Soil Sci. Soc. Am. J., 57, 1283–1288, https://doi.org/10.2136/sssaj1993.03615995005700050020x, 1993.

Hall, S. J., Berhe, A. A., and Thompson, A.: Order from disorder: do soil organic matter composition and turnover co-vary with iron phase crystallinity?, Biogeochemistry, 140, 93–110, https://doi.org/10.1007/s10533-018-0476-4, 2018.

Jamoteau, F., Cam, N., Levard, C., Doelsch, E., Gassier, G., Duvivier, A., Boulineau, A., Saint-Antonin, F., and Basile-Doelsch, I.: Structure and Chemical Composition of Soil C-Rich Al–Si–Fe Coprecipitates at Nanometer Scale, Environ. Sci. Technol., 57, 20615-26, https://doi.org/10.1021/acs.est.3c06557, 2023.

Jilling, A., Keiluweit, M., Gutknecht, J. L. M., and Grandy, A. S.: Priming mechanisms providing plants and microbes access to mineral-associated organic matter, Soil Biol. Biochem., 158, 108265, https://doi.org/10.1016/j.soilbio.2021.108265, 2021.

Just, C., Poeplau, C., Don, A., van Wesemael, B., Kögel-Knabner, I., and Wiesmeier, M.: A Simple Approach to Isolate Slow and Fast Cycling Organic Carbon Fractions in Central European Soils – Importance of Dispersion Method, Front. Soil Sci., 1, 13, https://doi.org/10.3389/fsoil.2021.692583, 2021.

Kaiser, K., Guggenberger, G., Haumaier, L., and Zech, W.: The composition of dissolved organic matter in forest soil solutions: changes induced by seasons and passage through the mineral soil, Org. Geochem., 33, 307–318, https://doi.org/10.1016/S0146-6380(01)00162-0, 2002.

Keiluweit, M., Bougoure, J. J., Nico, P. S., Pett-Ridge, J., Weber, P. K., and Kleber, M.: Mineral protection of soil carbon counteracted by root exudates, Nat. Clim. Change, 5, 588–595, https://doi.org/10.1038/nclimate2580, 2015.

Kinyangi, J., Solomon, D., Liang, B., Lerotic, M., Wirick, S., and Lehmann, J.: Nanoscale Biogeocomplexity of the Organomineral Assemblage in Soil, Soil Sci. Soc. Am. J., 70, 1708–1718, https://doi.org/10.2136/sssaj2005.0351, 2006.

Kleber, M., Mikutta, C., and Jahn, R.: Andosols in Germany – pedogenesis and properties, Catena, 56, 67–83, https://doi.org/10.1016/j.catena.2003.10.015, 2004.

Kleber, M., Eusterhues, K., Keiluweit, M., Mikutta, C., Mikutta, R., and Nico, P. S.: Chapter One – Mineral–Organic Associations: Formation, Properties, and Relevance in Soil Environments, in: Advances in Agronomy, edited by: Sparks, D. L., Academic Press, vol. 130, 1–140, https://doi.org/10.1016/bs.agron.2014.10.005, 2015.

Kleber, M., Bourg, I. C., Coward, E. K., Hansel, C. M., Myneni, S. C. B., and Nunan, N.: Dynamic interactions at the mineral–organic matter interface, Nat. Rev. Earth Environ., 2, 402–421, https://doi.org/10.1038/s43017-021-00162-y, 2021.

Koga, N., Shimoda, S., Shirato, Y., Kusaba, T., Shima, T., Niimi, H., Yamane, T., Wakabayashi, K., Niwa, K., Kohyama, K., Obara, H., Takata, Y., Kanda, T., Inoue, H., Ishizuka, S., Kaneko, S., Tsuruta, K., Hashimoto, S., Shinomiya, Y., Aizawa, S., Ito, E., Hashimoto, T., Morishita, T., Noguchi, K., Ono, K., Katayanagi, N., and Atsumi, K.: Assessing changes in soil carbon stocks after land use conversion from forest land to agricultural land in Japan, Geoderma, 377, 114487, https://doi.org/10.1016/j.geoderma.2020.114487, 2020.

Le Guillou, C., Bernard, S., De la Pena, F., and Le Brech, Y.: XANES-Based Quantification of Carbon Functional Group Concentrations, Anal. Chem., 90, 8379–8386, https://doi.org/10.1021/acs.analchem.8b00689, 2018.

Lehmann, J., Solomon, D., Kinyangi, J., Dathe, L., Wirick, S., and Jacobsen, C.: Spatial complexity of soil organic matter forms at nanometre scales, Nat. Geosci., 1, 238–242, https://doi.org/10.1038/ngeo155, 2008.

Lenhardt, K. R., Breitzke, H., Buntkowsky, G., Mikutta, C., and Rennert, T.: Interactions of dissolved organic matter with short-range ordered aluminosilicates by adsorption and co-precipitation, Geoderma, 423, 115960, https://doi.org/10.1016/j.geoderma.2022.115960, 2022.

Lenhardt, K. R., Stein, M., and Rennert, T.: Silicon Incorporation Reduces the Reactivity of Short-range Ordered Aluminosilicates Toward Organic Acids, Clays Clay Miner., 71, 416-29, https://doi.org/10.1007/s42860-023-00248-2, 2023.

Levard, C. and Basile Doelsch, I.: Geology and mineralogy of imogolite-type materials, in: Nanosized tubular clay minerals, Elsevier, Academic Press, np, vol. 7, https://doi.org/10.1016/B978-0-08-100293-3.00003-0, 2016.

Levard, C., Doelsch, E., Basile-Doelsch, I., Abidin, Z., Miche, H., Masion, A., Rose, J., Borschneck, D., and Bottero, J.-Y.: Structure and distribution of allophanes, imogolite and proto-imogolite in volcanic soils, Geoderma, 183–184, 100–108, https://doi.org/10.1016/j.geoderma.2012.03.015, 2012.

Li, H., Bölscher, T., Winnick, M., Tfaily, M. M., Cardon, Z. G., and Keiluweit, M.: Simple Plant and Microbial Exudates Destabilize Mineral-Associated Organic Matter via Multiple Pathways, Environ. Sci. Technol., 55, 3389–3398, https://doi.org/10.1021/acs.est.0c04592, 2017.

Lugato, E., Lavallee, J. M., Haddix, M. L., Panagos, P., and Cotrufo, M. F.: Different climate sensitivity of particulate and mineral-associated soil organic matter, Nat. Geosci., 14, 295–300, https://doi.org/10.1038/s41561-021-00744-x, 2021.

Lutfalla, S., Barré, P., Bernard, S., Le Guillou, C., Alléon, J., and Chenu, C.: Multidecadal persistence of organic matter in soils: multiscale investigations down to the submicron scale, Biogeosciences, 16, 1401–1410, https://doi.org/10.5194/bg-16-1401-2019, 2019.

Manderscheid, B. and Matzner, E.: Spatial heterogeneity of soil solution chemistry in a mature Norway spruce (Picea abies (L.) Karst.) stand, Water. Air. Soil Pollut., 85, 1185–1190, https://doi.org/10.1007/BF00477142, 1995.

Mimmo, T., Del Buono, D., Terzano, R., Tomasi, N., Vigani, G., Crecchio, C., Pinton, R., Zocchi, G., and Cesco, S.: Rhizospheric organic compounds in the soil–microorganism–plant system: their role in iron availability, Eur. J. Soil Sci., 65, 629–642, https://doi.org/10.1111/ejss.12158, 2014.

Newcomb, C. J., Qafoku, N. P., Grate, J. W., Bailey, V. L., and Yoreo, J. J. D.: Developing a molecular picture of soil organic matter–mineral interactions by quantifying organo–mineral binding, Nat. Commun., 8, 396, https://doi.org/10.1038/s41467-017-00407-9, 2017.

Osher, L. J., Matson, P. A., and Amundson, R.: Effect of land use change on soil carbon in Hawaii, Biogeochemistry, 65, 213–232, https://doi.org/10.1023/A:1026048612540, 2003.

Pansu, M. and Gautheyrou, J. (Eds.): Mineralogical Separation by Selective Dissolution, in: Handbook of Soil Analysis: Mineralogical, Organic and Inorganic Methods, Springer Berlin Heidelberg, Berlin, Heidelberg, 167–219, https://doi.org/10.1007/978-3-540-31211-6_6, 2006.

Parfitt, R. L.: Allophane and imogolite: role in soil biogeochemical processes, Clay Miner., 44, 135–155, https://doi.org/10.1180/claymin.2009.044.1.135, 2009.

Poeplau, C. and Don, A.: Sensitivity of soil organic carbon stocks and fractions to different land-use changes across Europe, Geoderma, 192, 189–201, https://doi.org/10.1016/j.geoderma.2012.08.003, 2013.

Poeplau, C., Vos, C., and Don, A.: Soil organic carbon stocks are systematically overestimated by misuse of the parameters bulk density and rock fragment content, SOIL, 3, 61–66, https://doi.org/10.5194/soil-3-61-2017, 2017.

Quéro, S., Hatté, C., Cornu, S., Duvivier, A., Cam, N., Jamoteau, F., Borschneck, D., and Basile-Doelsch, I.: Dynamics of carbon loss from an Arenosol by a forest to vineyard land use change on a centennial scale, SOIL, 8, 517–539, https://doi.org/10.5194/soil-8-517-2022, 2022.

Rasmussen, C., Heckman, K., Wieder, W. R., Keiluweit, M., Lawrence, C. R., Berhe, A. A., Blankinship, J. C., Crow, S. E., Druhan, J. L., Hicks Pries, C. E., Marin-Spiotta, E., Plante, A. F., Schädel, C., Schimel, J. P., Sierra, C. A., Thompson, A., and Wagai, R.: Beyond clay: towards an improved set of variables for predicting soil organic matter content, Biogeochemistry, 137, 297–306, https://doi.org/10.1007/s10533-018-0424-3, 2018.

Ravel, B. and Newville, M.: ATHENA, ARTEMIS, HEPHAESTUS: data analysis for X-ray absorption spectroscopy using IFEFFIT, J. Synchrotron Radiat., 12, 537–541, https://doi.org/10.1107/S0909049505012719, 2005.

Rennert, T.: Wet-chemical extractions to characterise pedogenic Al and Fe species – a critical review, Soil Res., 57, 1–16, https://doi.org/10.1071/SR18299, 2018.

Rennert, T. and Lenhardt, K. R.: Potential pitfalls when using popular chemical extractions to characterize Al- and Fe-containing soil constituents, J. Plant Nutr. Soil Sci., 1–12, https://doi.org/10.1002/jpln.202300268, 2024.

Sanderman, J., Hengl, T., and Fiske, G.: Soil carbon debt of 12,000 years of human land use, P. Natl. Acad. Sci. USA, 114, 9575-9580, https://doi.org/10.1073/pnas.1706103114, 2017.

Schmidt, M. A., Gonzalez, J. M., Halvorson, J. J., and Hagerman, A. E.: Metal mobilization in soil by two structurally defined polyphenols, Chemosphere, 90, 1870–1877, https://doi.org/10.1016/j.chemosphere.2012.10.010, 2013.

Shimada, H., Wagai, R., Inoue, Y., Tamura, K., and Asano, M.: Millennium timescale carbon stability in an Andisol: How persistent are organo-metal complexes?, Geoderma, 417, 115820, https://doi.org/10.1016/j.geoderma.2022.115820, 2022.

Solomon, D., Lehmann, J., Kinyangi, J., Amelung, W., Lobe, I., Pell, A., Riha, S., Ngoze, S., Verchot, L., Mbugua, D., Skjemstad, J., and Schäfer, T.: Long-term impacts of anthropogenic perturbations on dynamics and speciation of organic carbon in tropical forest and subtropical grassland ecosystems, Glob. Change Biol., 13, 511–530, https://doi.org/10.1111/j.1365-2486.2006.01304.x, 2007.

Solomon, D., Lehmann, J., Harden, J., Wang, J., Kinyangi, J., Heymann, K., Karunakaran, C., Lu, Y., Wirick, S., and Jacobsen, C.: Micro- and nano-environments of carbon sequestration: Multi-element STXM–NEXAFS spectromicroscopy assessment of microbial carbon and mineral associations, Chem. Geol., 329, 53–73, https://doi.org/10.1016/j.chemgeo.2012.02.002, 2012.

Strobel, B. W., Hansen, H. C. B., Borggaard, O. K., Andersen, M. K., and Raulund-Rasmussen, K.: Composition and reactivity of DOC in forest floor soil solutions in relation to tree species and soil type, Biogeochemistry, 56, 1–26, https://doi.org/10.1023/A:1011934929379, 2001.

Tamm, O.: Eine Methode zur Bestim mung der anorganischen Komponenten des Gelkomplexes im Boden, Medd. Fran Statens Skogsforsoksanstalt, 19, 385–404, 1922.

Tamrat, W. Z., Rose, J., Grauby, O., Doelsch, E., Levard, C., Chaurand, P., and Basile-Doelsch, I.: Composition and molecular scale structure of nanophases formed by precipitation of biotite weathering products, Geochim. Cosmochim. Ac., 229, 53–64, https://doi.org/10.1016/j.gca.2018.03.012, 2018.

Tamrat, W. Z., Rose, J., Grauby, O., Doelsch, E., Levard, C., Chaurand, P., and Basile-Doelsch, I.: Soil organo-mineral associations formed by co-precipitation of Fe, Si and Al in presence of organic ligands, Geochim. Cosmochim. Ac., 260, 15–28, https://doi.org/10.1016/j.gca.2019.05.043, 2019.

Trumbore, S. E., Vogel, J. S., and Southon, J. R.: AMS 14C Measurements of Fractionated Soil Organic Matter: An Approach to Deciphering the Soil Carbon Cycle, Radiocarbon, 31, 644–654, https://doi.org/10.1017/S0033822200012248, 1989.

Uroz, S., Calvaruso, C., Turpault, M.-P., and Frey-Klett, P.: Mineral weathering by bacteria: ecology, actors and mechanisms, Trends Microbiol., 17, 378–387, https://doi.org/10.1016/j.tim.2009.05.004, 2009.

Verde, J. R., Arbestain, M. C., and Macías, F.: Expression of andic properties in soils from Galicia (NW Spain) under forest and agricultural use, Eur. J. Soil Sci., 56, 53–64, https://doi.org/10.1111/j.1351-0754.2004.00651.x, 2005.

Wada, K.: The Distinctive Properties of Andosols, in: Advances in Soil Science, edited by: Stewart, B. A., New York, NY, Springer, 173–229, https://doi.org/10.1007/978-1-4612-5088-3_4, 1985.

Wada, K. and Harward, M. E.: Amorphous Clay Constituents of Soils, in: Advances in Agronomy, edited by: Brady, N. C., Academic Press, vol. 26, 211–260, https://doi.org/10.1016/S0065-2113(08)60872-X, 1974.

Wagai, R. and Mayer, L. M.: Sorptive stabilization of organic matter in soils by hydrous iron oxides, Geochim. Cosmochim. Ac., 71, 25–35, https://doi.org/10.1016/j.gca.2006.08.047, 2007.

Wagai, R., Kajiura, M., Uchida, M., and Asano, M.: Distinctive Roles of Two Aggregate Binding Agents in Allophanic Andisols: Young Carbon and Poorly-Crystalline Metal Phases with Old Carbon, Soil Syst., 2, 29, https://doi.org/10.3390/soilsystems2020029, 2018.

Wan, J., Tyliszczak, T., and Tokunaga, T. K.: Organic carbon distribution, speciation, and elemental correlations within soil microaggregates: Applications of STXM and NEXAFS spectroscopy, Geochim. Cosmochim. Ac., 71, 5439–5449, https://doi.org/10.1016/j.gca.2007.07.030, 2007.